Simultaneous Visualization of the Thoracic Duct and Blood Vessels Using MRI: A Comparison Between Balanced Turbo-field-echo and Spin-echo

Xuyang SUN[*1], Tetsu NIWA[*1], Takakiyo NOMURA[*1], Susumu TAKANO[*2], Kento YOKOYAMA[*1], Kotaro IWATA[*1], Sadanori KAMEDA[*1], Hiroki KOBAYASHI[*1], Takuya HARA[*1,3] and Jun HASHIMOTO[*1]

[*1]*Department of Diagnostic Radiology, Tokai University School of Medicine*
[*2]*Department of Radiology, Tokai University Hospital*
[*3]*Current affiliation: Department of Radiology, Isehara Kyodo Hospital*

(Received April 13, 2023; Accepted June 26, 2023)

Objective: Magnetic resonance thoracic ductography (MRTD), concomitant with blood vessel imaging, provides useful anatomical information. The purpose of this study was to assess the visibility of the thoracic duct and blood vessels simultaneously by MRTD using balanced turbo-field-echo (bTFE) and turbo spin-echo (TSE).
Methods: MRTDs concomitant with blood vessel imaging on bTFE and TSE were obtained for 10 healthy volunteers with a 1.5T-magnetic resonance unit. Visibility of the thoracic duct, blood vessels in the thoracic region; motion artifacts; and overall image quality were scored by two radiologists using three-to-five-point scales; those were compared between bTFE and TSE.
Results: The thoracic duct was generally well-visualized on MRTD sequences. The upper part of the thoracic duct was better visualized on TSE than on bTFE ($p < 0.05$). The blood vessels were well visualized on bTFE and TSE; the bilateral subclavian arteries and the right subclavian veins were better visualized on TSE than on bTFE (all $p < 0.05$). Motion artifacts and overall image quality were better on TSE than on bTFE ($p = 0.0039$ and 0.0020, respectively).
Conclusion: MRTD concomitant with blood vessel imaging on TSE has better visibility of the thoracic duct and blood vessels than bTFE.

Key words: blood vessel, magnetic resonance imaging, magnetic resonance thoracic ductography, thoracic duct, thora

INTRODUCTION

The thoracic duct is the largest lymphatic vessel in the human body. Its total length is approximately 35–40 cm [1]. The thoracic duct ascends from the cisterna chyli, which receives bilateral lumbar and intestinal lymphatic trunks. Generally, the thoracic duct enters the thoracic cavity through the phrenic aortic hiatus and ascends between the thoracic aorta and the azygos vein along the anterior side of the spine to the back of the oesophagus, and curves leftward in the middle, upper the thoracic cavity. It connects in an arc to the left venous angle [2].

Injury to the thoracic duct can occur during thoracic surgery, such as during esophagectomy in patients with oesophageal cancer. This can lead to a serious complication, chylothorax, a state in which lymph leaks into the pleural cavity. During surgery, avoiding intraoperative and postoperative complications is essential.

To avoid complications, it is necessary to correctly grasp the course of the thoracic duct before surgery since anatomical variations of the thoracic duct are known [2–7]. Lymphatic vessels mainly contain lymph (tissue fluid)[8]; thus, lymphography can be performed by a technique of magnetic resonance (MR) hydrography called MR thoracic ductography (MRTD) [9–11]. MRTD is useful, particularly before thoracic surgery, to prevent chylothorax [7, 12]. MRTD has been obtained by heavily T2-weighted imaging with emphasis on the liquid component and suppressing signals other than liquid [9, 10]. In addition, MRTD, concomitant with blood vessel imaging, provides further anatomical information using a balanced turbo-field-echo (bTFE) sequence [13, 14]. bTFE has an excellent time resolution and good contrast resolution, obtained with the water being stationary and the blood flowing, due to its high T2/T1 ratio [15]. Thus, bTFE can provide good MRTD with blood vessel imaging in a relatively short time. However, a potential disadvantage of bTFE is its susceptibility, etching, banding, and fringe artifacts [16]. Spin-echo (SE) imaging is another method for visualizing the thoracic duct. SE imaging usually displays the blood vessels as a flow void; however bright-vessel imaging can be obtained by reducing the echo train spacing on a turbo SE (TSE) (or fast SE) sequence [17–19]. Therefore, we postulate that TSE imaging could be an alternative method for MRTD with simultaneous blood vessel imaging. MRTD itself is an established method using heavily T2-weighted imaging [9–11]; however, simultaneous visualization of the

Tetsu NIWA, Department of Diagnostic Radiology, Tokai University School of Medicine, 143 Shimokasuya, Isehara, Kanagawa 259-1193, Japan
Tel: +81-463-93-1121 Fax: +81-463-93-6827 E-mail: niwat@tokai-u.jp

thoracic duct and the blood vessels using bTFE and TSE is not well understood. In this study, we aimed to compare the visibility of MRTD with the simultaneous visualization of blood vessels using bTFE and TSE sequences.

MATERIALS AND METHODS

Participants

This study was approved by the ethics committee of our institution (the Institutional Review Board for Clinical Research, Tokai University, No. 21R320), and written informed consent was obtained from all participants. The investigation conforms with the principles outlined in the Declaration of Helsinki. Ten healthy volunteers (eight men and two women; mean age, 33.8 years [range, 25–52 years]) were recruited for this study.

MR imaging

MRTD concomitant with blood vessel imaging was performed using a 1.5-T MR unit (Ambition, Philips, Best, The Netherlands). A 16-channel, receive-only body torso coil was used to cover the thoracic region. The scanning area comprised a slight oblique coronal plane at the cranial portion anteriorly and the caudal portion posteriorly to cover the entire thoracic duct in the chest region. MRTDs with simultaneous visualization of the blood vessels were obtained using bTFE and TSE with the following parameters: bTFE, signal readout = three-dimensional (3D) TFE, repetition time (TR)/echo time (TE) = 5.7/2.9 ms, and flip angle = 120 degrees; TSE, signal readout = 3D TSE, TR/TE = 991/274 ms, and flip angle = 90 degrees. Conventional heavily T2-weighted imaging was also performed to compare the thoracic duct visibility with following parameters: signal readout = 3D TSE, TR/TE = 3000/600 ms, and flip angle = 90 degrees. All other parameters were the same among the sequences: field of view = 300 × 300 mm, matrix = 288 × 288, slice thickness = 1.6 mm, number of slices = 120, turbo factor = 125, fat suppression = spectral presaturation with inversion recovery, and compressed sensing-sensitivity encoding (CS-SENSE) acceleration factor = 3. We used three-dimensional non-selective radiofrequency pulses for TSE to minimize echo train spacing (4.4 ms) to visualize the blood vessels. MRTDs were scanned using bellows-based respiratory gating. A cardiac gating was not used to avoid longer acquisition times.

Image assessment

Visibility of the thoracic duct and blood vessels, and image quality were evaluated by two board-certified radiologists with 9 and 25 years of experience in thoracic radiology, respectively. The visibility of the thoracic duct was compared between bTFE, TSE, and heavily T2-weighted imaging. Due to the poor visibility of the blood vessels on heavily T2-weighted imaging, blood vessel visibility was compared between bTFE and TSE.

For assessment of the thoracic duct, the main thoracic duct was trisected as follows: upper, the portion above the bronchial bifurcation level; middle, the upper half from the bronchial bifurcation level to the diaphragm level; and lower, the lower half from the bronchial bifurcation level to the diaphragm level. The visibility of each segment of the thoracic duct was scored on bTFE, TSE, and heavily T2-weighted images as follows: 0 = no visualization; 1 = partial visualization (partially visualized thoracic duct, but most of the thoracic duct is not visible); 2 = moderate visualization (approximately half of the thoracic duct is visualized); 3 = good visualization (most of the thoracic duct is visualized, but it is partially impossible to identify the continuity of the thoracic duct); and 4 = complete visualization (no discontinuity of the thoracic duct). The visibility of the thoracic duct termination into the venous system was assessed on bTFE and TSE using the following scores: 0 = uncertain; 1 = somewhat certain (slightly less visibility of the draining portion or slightly less visibility of the continuity from the main thoracic duct); and 2 = absolutely certain. The blood vessels' visibility was assessed on bTFE and TSE regarding the arteries, including the ascending aorta, aortic arch, and descending aorta, brachiocephalic artery, bilateral common carotid arteries, and subclavian arteries, and the veins including the superior and inferior vena cava, bilateral brachiocephalic vein, internal carotid veins, subclavian veins, azygous veins, and azygous arch. The same criteria as those used for thoracic duct visibility were used for the blood vessels assessment. Finally, image quality regarding motion artifacts and overall image quality were assessed using bTFE and TSE. Motion artifacts were scored as follows: 0 = severe artifact (anatomy cannot be interpreted); 1 = moderate artifact (anatomical structures were obscured but identifiable); 2 = mild artifact (some artifact, but most anatomical structures were identifiable); 3 = slight artifact (trace artifact); and 4 = no artifact. The overall image quality was scored as 0 = non-diagnostic; 1 = limited but interpretable; 2 = minimally limited; and 3 = optimal quality.

Representative images were shown with curved multiplanar reformation and partial maximum intensity projection.

Statistical analysis

The scores between the two readers were averaged and used for statistical analysis; the differences in scores between the two readers were calculated. The scan times and the assessed scores for visibility of the thoracic duct were compared among bTFE, TSE, and heavily T2-weighted imaging using the Friedman test with post hoc pairwise comparison. The visibility of the thoracic duct termination into the venous system and the blood vessels, and image quality were compared between bTFE and TSE using the Wilcoxon test. Statistical analysis was performed using MedCalc Statistical Software version 20.112 (MedCalc Software Ltd., Ostend, Belgium; https://www.medcalc.org; 2022). *P*-values < 0.05 were considered statistically significant.

RESULTS

The scan times of MRTD with bTFE (mean [range], 230 [184–318] s), TSE (306 [235–348] s), and heavily T2-weighted imaging (253 [236–318] s) were significantly different ($p = 0.006$), and post hoc tests revealed that the scan time with bTFE was significantly shorter than that with TSE and heavily T2-weighted ($p < 0.05$).

The differences in the scores for each assessed issue between the two readers were less than one (mean

Table 1 Scores for the visibility of the thoracic duct of each portion with balanced turbo-field echo, turbo spin-echo, and heavily T2-weighted imaging

Thoracic duct	bTFE[†]	TSE[‡]	Heavily T2-weighted imaging	*p*
Upper (0–4)[¶]	3.5 (2.5–4)	4 (3–4)	4 (2.5–4)	< 0.0001[*]
Middle (0–4)[¶]	4 (3.5–4)	4 (3.5–4)	3.75 (2.5–4)	0.068
Lover (0–4)[¶]	4 (3.5–4)	4 (4)	4 (1.5–4)	0.014[**]
Thoracic duct termination into the venous system (0–2)[†]	2 (2)	2 (2)	NA[§]	NA

[†]bTFE, balanced turbo field-echo; [‡]TSE, turbo spin-echo; [§]NA, not applicable

Data are presented as median (range); [¶]Parenthesis is the range of scores;

[*]The scores for TSE were higher than those for bTFE in the post hoc test ($p < 0.05$);

[**]The scores for bTFE and TSE were higher than those for heavily T2-weighted imaging in post hoc tests ($p < 0.05$).

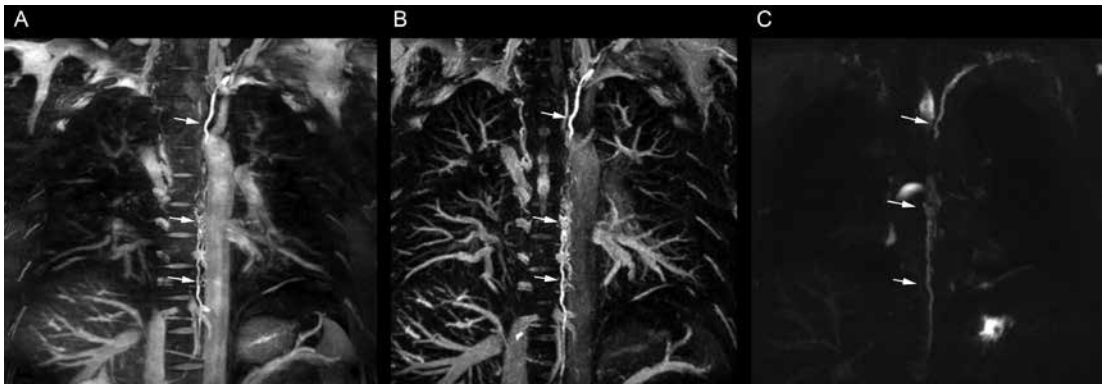

Fig. 1 Magnetic resonance thoracic ductography (MRTD) concomitant with blood vessel imaging in a 29-year-old man. MR images with curved multiplanar reformations with partial maximum intensity projection well visualize thoracic duct (arrows) on balanced turbo-field-echo (A), turbo spin-echo (B), and heavily T2-weighted imaging (C). Note that stitch formation of the middle portion of thoracic duct is well demonstrated on each MRTD.

Fig. 2 Visibility of the thoracic duct termination into the venous system on magnetic resonance thoracic ductography (MRTD) concomitant with blood vessel imaging in a 37-year-old man. MR images with partial maximum intensity projection well demonstrate the thoracic duct into the jugulovenous angle (arrows) on both balanced turbo-field-echo (A) and turbo spin-echo (B). I: internal jugular vein; S: subclavian vein.

difference, 0.015 ± 0.14). Table 1 presents the scores for each thoracic duct portion of the three MRTD sequences. Visibility of the thoracic duct was generally good for each assessed portion (median score, range 3.5–4; Fig. 1). Regarding the upper portion of the thoracic duct, scores of bTFE (median [range], 3.5 [2.5–4]), TSE (4 [3–4]), and heavily T2-weighted imaging (4 [2.5–4]) were significantly different ($p < 0.0001$), and post hoc tests revealed that the scores for TSE were higher than those for bTFE ($p < 0.05$). Regarding the middle portion of the thoracic duct, the scores of bTFE (4 [3.5–4]), TSE (4 [3.5–4]), and heavily T2-weighted imaging (3.75 [2.5–4]) were not significantly different ($p = 0.068$). Regarding the lower portion of the thoracic duct, the scores of bTFE (4 [3.5–4]), TSE (4 [4]), and heavily T2-weighted imaging (4 [1.5–4]) were significantly different ($p = 0.014$), and post hoc tests revealed that the scores for bTFE and TSE were higher than those for heavily T2-weighted imaging ($p < 0.05$). Visibility of the thoracic duct into the venous system was well-recognized for bTFE and TSE (all scores were 2 for both sequences, Fig. 2).

The visibility of blood vessels was assessed using bTFE and TSE (Table 2). Regarding the visibility of

Table 2 Scores for the visibility of the blood vessels with balanced turbo-field echo and turbo spin-echo

Assessed vessels	bTFE[†]	TSE[‡]	*p*
Artery (0–4)[‡‡]			
Ascending aorta	4 (4)	4 (4)	NA[§]
Aortic arch	4 (4)	4 (4)	NA
Descending aorta	4 (4)	4 (4)	NA
Brachiocephalic	4 (4)	4 (4)	NA
R[¶] common carotid	4 (4)	4 (4)	NA
L[††] common carotid	4 (4)	4 (4)	NA
R subclavian	3.25 (3–4)	4 (3–4)	0.023[*]
L subclavian	3 (3–4)	4 (4)	0.0039[*]
Vein (0–4)[‡‡]			
Superior vena cava	4 (4)	4 (4)	NA
Inferior vena cava	4 (3.5–4)	4(3–4)	NA
R brachiocephalic	4 (4)	4 (4)	NA
L brachiocephalic	4 (4)	4 (4)	NA
R internal carotid	4 (3.5–4)	4 (4)	NA
L internal carotid	4 (3.5–4)	4 (4)	NA
R subclavian	3.5 (1.5–4)	4 (3.5–4)	0.046[*]
L subclavian	4 (3.5–4)	4 (4)	NA
Azygous	3.75 (3–4)	3.5 (3–4)	0.84
Azygous arch	3.5 (3–4)	4 (3.5–4)	0.25

[†]bTFE, balanced turbo field-echo; [‡]TSE, turbo spin-echo; [§]NA, not applicable; [¶]R, right; [††]L, left

Data are presented as median (range); [‡‡]Parenthesis is the range of scores; [*]The scores for the bilateral subclavian arteries and those for right subclavian veins with bTFE were lower than those with TSE, respectively.

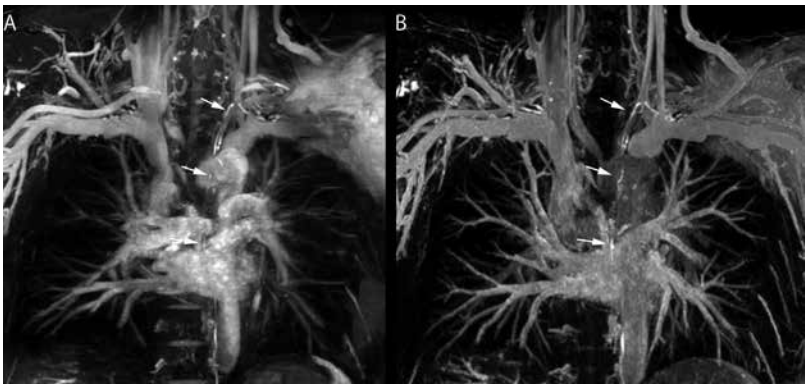

Fig. 3 Visibility of the blood vessels on magnetic resonance thoracic ductography (MRTD) in a 52-year-old man. MR images with partial maximum intensity projection generally well demonstrate both thoracic duct (arrows) and the major blood vessels on both balanced turbo-field-echo (A) and turbo spin-echo TSE (B).

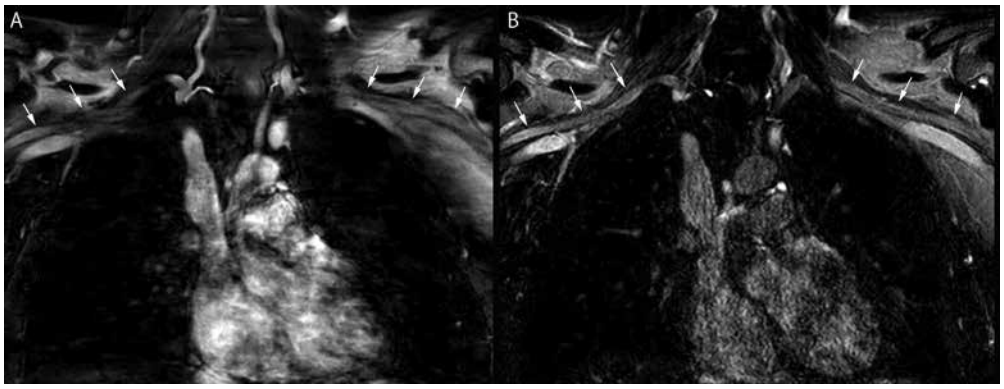

Fig. 4 Visibility of the subclavian arteries on magnetic resonance thoracic ductography (MRTD) concomitant with blood vessel imaging in a 25-year-old man. The bilateral subclavian arteries (arrows) are less demonstrated with balanced turbo-field-echo (A), compared with turbo spin-echo (B).

Table 3 Scores for artifact and image quality with balanced turbo-field echo and turbo spin-echo

Factor	bTFE[†]	TSE[‡]	*p*
Motion artifacts (0–4)[§]	2 (2–2.5)	3 (2.5–3)	0.0039[*]
Overall image quality (0–3)[§]	2 (1.5–2)	3 (2–3)	0.0020[**]

[†]bTFE, balanced turbo field-echo; [‡]TSE, turbo spin-echo
Data are presented as median (range); [§]Parenthesis is the range of scores;
[*]The scores for motion artifact with bTFE were lower than those with TSE.
[**]The scores for overall image quality were lower than those with TSE.

the arteries, all the assessed arteries were generally well visualized (median scores, 3–4; Fig. 3); bilateral subclavian arteries were rated lower for bTFE than for TSE (right subclavian artery, median score, 3.25 vs. 4, $p = 0.023$; left subclavian artery, median score, 3 vs. 4, $p = 0.0039$; Fig. 4). Regarding the visibility of the veins, all the assessed veins were generally well visualized (median scores, 3.5–4), except the right subclavian vein with bTFE; the right subclavian veins were rated lower with bTFE than with TSE (median score, 3.5 vs. 4, $p = 0.046$).

The scores for motion artifacts and overall image quality differed significantly between the bTFE and TSE groups (Table 3). The scores for motion artifacts with bTFE (median score [range], 2 [2–2.5]) were lower than those with TSE (3 [2.5–3]) ($p = 0.0039$). The scores for overall image quality with bTFE (median score [range], 2 [1.5–2]) were lower than those with TSE (3 [2–3]) ($p = 0.0020$).

DISCUSSION

We discovered relatively good visibility of the thoracic duct with bTFE and TSE; they were generally comparable and had better visibility of the thoracic duct than heavily T2-weighted imaging. Thus, bTFE and TSE sequences can be alternative methods of MRTD for heavily T2-weighted imaging. Regarding the lower part of the thoracic duct, bTFE and TSE achieved better visibility than heavy T2-weighted imaging. This may be because half-Fourier imaging on heavily T2-weighted images might result in blurring of the structures in some cases. MR hydrography has been applied to cholangiopancreatography and urography, where bTFE has been reported to have good visibility [20–22]. However, the differences between bTFE and TSE in MRTD are poorly understood. In this study, the visibility of the upper part of the thoracic duct was better with TSE than with bTFE. This may be due to the susceptibility artifact on bTFE since the upper part of the thoracic duct runs close to the lungs. The visibility of the other portions of the thoracic duct was generally comparable between bTFE and TSE.

Simultaneous visualization of the blood vessels offers an advantage in MRTD over conventional heavily T2-weighted imaging, such as grasping the anatomical location and relation to the surrounding structures of the thoracic duct [13]. Visualization of the blood vessels on bTFE is based on fully balanced gradients without spoiling the transverse magnetization [15]. bTFE visualizes all blood in the imaging slab, regardless of its source or flow velocity [19]. Reportedly, bTFE provided good visibility for arteries and veins [15, 16, 23–25]. In this study, bTFE was used to visualize the main thoracic blood vessels; however, the subclavian vessels were visualized less on bTFE than on TSE, possibly due to susceptibility artifacts or inhomogeneous fat-suppression effects of bTFE [26]. Concurrently, vessel imaging using TSE has also been introduced [18, 27]. Generally, bright-vessel imaging on TSE can be achieved by reducing the echo spacing time, resulting in a short acquisition time. In this state, motion-related artifacts effectively freeze [17], enabling the visualization of flowing blood vessels. Bright-vessel imaging of the arteries can be obtained on TSE during the diastolic phase, where the arterial flow is relatively slow. In contrast, the arterial signal during the systolic phase is dark, particularly in arteries with fast flow, such as the great vessels in the thorax [19]. In this study, we did not use cardiac gating to reduce scan time. Therefore, the signals of the arteries with TSE were the result of averaged signals of the systolic and diastolic phases. As a result, the signals of the artery decreased compared to those of the veins. However, most of the vessels in the thoracic region were recognizable despite some reduction in the arterial signals. Furthermore, for the subclavian region, TSE had better visibility than bTFE, which may be due to fewer artifacts in TSE. Thus, TSE in combination with MRTD is considered to provide good visibility of blood vessels in the thoracic region.

The scan time of bTFE was shorter than that of TSE and heavily T2-weighted imaging in our study, which is valuable for MRTD application to clinical practice. The visibility of the thoracic duct and the blood vessels were slightly lower with bTFE than with TSE; however, bTFE use is advantageous when scanning time is crucial. Another factor that affects the scanning time is the gating method. We only used respiratory gating in this study; however, cardiac gating is an option for MRTD [28]. Since relatively good visibility of the thoracic duct was obtained for the bTFE and TSE sequences, we assume that cardiac gating is not mandatory for MRTD.

Motion artifacts and overall image quality were better on TSE than on bTFE, which may be due to fewer artifacts on TSE: bTFE tends to be affected by susceptibility and banding artifact [16], resulting in blurring or less visibility in some regions. In addition, setting a short echo train spacing to visualize blood vessels on TSE may contribute to reducing motion artifacts. In this study, respiratory gating was used; however, the MR images were not free from thoracic motion. In addition, cardiac movement causes some motion artifacts. Due to the magnetic inhomogeneity and physiological motion of the thoracic region, TSE may have better image quality. TSE should provide a stable imaging quality, although it requires a longer scan time.

This study had several limitations. First, the sample size was small, and all the participants were healthy volunteers. Our MRTD sequences should be evaluated in a larger number of patients. Second, a qualitative image assessment was performed. Thus, the scores may contain subjective variations; however, the differ-

ences in the scores between the two readers were small. Readers' agreement could not be calculated because of an imbalance in the frequency of the scores. Third, there were no references to the thoracic duct or blood vessels. We only compared individual visibility between the sequences. Fourth, both the thoracic duct and blood vessels are displayed as hypersignal structures on bTFE and TSE. Therefore, tiny branches may be difficult to differentiate. However, major vessels are distinguishable based on their anatomical location and continuity on imaging slices. In our series, there were no cases in which we could not differentiate the blood vessels from thoracic duct.

In conclusion, simultaneous visualization of the thoracic duct and blood vessels can be achieved using bTFE and TSE. MRTD concomitant with bold vessel imaging on TSE may have better visibility of the thoracic duct and blood vessels and better imaging quality than bTFE. TSE may provide a stable imaging quality for thoracic duct and blood vessel visualization as a preoperative evaluation.

REFERENCES

1) P B, Yalakurthi S, Vishnumukkala T, Dorai Raj SJ. Anatomical variations of the human thoracic duct. IJAR 2018; 6: 5861–5868.
2) Phang K, Bowman M, Phillips A, Windsor J. Review of thoracic duct anatomical variations and clinical implications. Clin Anat 2014; 27: 637–644.
3) Okuda I, Udagawa H, Takahashi J, Yamase H, Kohno T, Nakajima Y. Magnetic resonance-thoracic ductography: imaging aid for thoracic surgery and thoracic duct depiction based on embryological considerations. Gen Thorac Cardiovasc Surg 2009; 57: 640–646.
4) Okuda I, Udagawa H, Hirata K, Nakajima Y. Depiction of the thoracic duct by magnetic resonance imaging: comparison between magnetic resonance imaging and the anatomical literature. Jpn J Radiol 2011; 29: 39–45.
5) Inoue M, Nakatsuka S, Yashiro H, Tamura M, Suyama Y, Tsukada J, *et al*. Lymphatic intervention for various types of lymphorrhea: access and treatment. Radiographics 2016; 36: 2199–2211.
6) Johnson OW, Chick JF, Chauhan NR, Fairchild AH, Fan CM, Stecker MS, *et al*. The thoracic duct: clinical importance, anatomic variation, imaging, and embolization. Eur Radiol 2016; 26: 2482–2493.
7) Higuchi T, Ozawa S, Koyanagi K, Oguma J, Ninomiya Y, Yatabe K, *et al*. Clinical impacts of magnetic resonance thoracic ductography on preventing postoperative chylothorax after thoracoscopic esophagectomy for esophageal cancer. Esophagus 2021; 18: 753–763.
8) Robinson CL. The management of chylothorax. Ann Thorac Surg 1985; 39: 90–95.
9) Hayashi S, Miyazaki M. Thoracic duct: visualization at nonenhanced MR lymphography--initial experience. Radiology 1999; 212: 598–600.
10) Matsushima S, Ichiba N, Hayashi D, Fukuda K. Nonenhanced magnetic resonance lymphoductography: visualization of lymphatic system of the trunk on 3-dimensional heavily T2-weighted image with 2-dimensional prospective acquisition and correction. J Comput Assist Tomogr 2007; 31: 299–302.
11) Chavhan GB, Amaral JG, Temple M, Itkin M. MR lymphangiography in children: technique and potential applications. RadioGraphics 2017; 37: 1775–1790.
12) Oguma J, Ozawa S, Kazuno A, Nitta M, Ninomiya Y, Yatabe K, *et al*. Clinical significance of new magnetic resonance thoracic ductography before thoracoscopic esophagectomy for esophageal cancer. World J Surg 2018; 42: 1779–1786.
13) Kato T, Takase K, Ichikawa H, Satomi S, Takahashi S. Thoracic duct visualization: combined use of multidetector-row computed tomography and magnetic resonance imaging. J Comput Assist Tomogr 2011; 35: 260–265.
14) Pabon-Ramos WM, Raman V, Schwartz FR, Tong BC, Koweek LM. Magnetic resonance lymphangiography of the central lymphatic system: technique and clinical applications. J Magn Reson Imaging 2021; 53: 374–380.
15) Sumi T, Sumi M, Van Cauteren M, Kimura Y, Nakamura T. Parallel imaging technique for the external carotid artery and its branches: comparison of balanced turbo field echo, phase contrast, and time-of-flight sequences. J Magn Reson Imaging 2007; 25: 1028–1034.
16) Schieda N, Isupov I, Chung A, Coffey N, Avruch L. Practical applications of balanced steady-state free-precession (bSSFP) imaging in the abdomen and pelvis. J Magn Reson Imaging 2017; 45: 11–20.
17) Miyazaki M, Sugiura S, Tateishi F, Wada H, Kassai Y, Abe H. Non-contrast-enhanced MR angiography using 3D ECG-synchronized half-Fourier fast spin echo. J Magn Reson Imaging 2000; 12: 776–783.
18) Miyazaki M, Takai H, Sugiura S, Wada H, Kuwahara R, Urata J. Peripheral MR angiography: separation of arteries from veins with flow-spoiled gradient pulses in electrocardiography-triggered three-dimensional half-Fourier fast spin-echo imaging. Radiology 2003; 227: 890–896.
19) Wheaton AJ, Miyazaki M. Non-contrast enhanced MR angiography: physical principles. J Magn Reson Imaging 2012; 36: 286–304.
20) Itatani R, Namimoto T, Atsuji S, Katahira K, Yamashita Y. Clinical application of navigator-gated three-dimensional balanced turbo-field-echo magnetic resonance cholangiopancreatography at 3 T: prospective intraindividual comparison with 1.5 T. Abdom Radiol (NY) 2016; 41: 1285–1292.
21) Çifçi E, Çoban G, Çiçek T, Gönülalan U. The diagnostic value of magnetic resonance urography using a balanced turbo field echo sequence. Eur Radiol 2016; 26: 4624–4631.
22) Jara H, Barish MA, Yucel EK, Melhem ER, Hussain S, Ferrucci JT. MR hydrography: theory and practice of static fluid imaging. AJR Am J Roentgenol 1998; 170: 873–882.
23) Gupta N, Swaminathan SV, DeMarco JK. Initial experience with balanced turbo field echo in depicting carotid artery stenosis: comparison with multiple overlapping thin slab acquisition and 3D contrast-enhanced magnetic resonance angiography. J Magn Reson Imaging 2005; 22: 354–360.
24) Enden T, Storås TH, Negård A, Haig Y, Sandvik L, Gjesdal KI, *et al*. Visualization of deep veins and detection of deep vein thrombosis (DVT) with balanced turbo field echo (b-TFE) and contrast-enhanced T1 fast field echo (CE-FFE) using a blood pool agent (BPA). J Magn Reson Imaging 2010; 31: 416–424.
25) Koizumi J, Horie T, Muro I, Kimura E, Shimizu K, Orii M, *et al*. Magnetic resonance venography of the lower limb. Int Angiol 2007; 26: 171–182.
26) Axel L, Kolman L, Charafeddine R, Hwang SN, Stolpen AH. Origin of a signal intensity loss artifact in fat-saturation MR imaging. Radiology 2000; 217: 911–915.
27) Nakamura K, Miyazaki M, Kuroki K, Yamamoto A, Hiramine A, Admiraal-Behloul F. Noncontrast-enhanced peripheral MRA: technical optimization of flow-spoiled fresh blood imaging for screening peripheral arterial diseases. Magn Reson Med 2011; 65: 595–602.
28) Kammerer FJ, Schlude B, Kuefner MA, Schlechtweg P, Hammon M, Uder M, *et al*. Morphology of the distal thoracic duct and the right lymphatic duct in different head and neck pathologies: an imaging based study. Head Face Med 2016; 12: 15.